Mustansiriyah Journal of Pure and Applied Sciences

www.MJPAS.com

The Influence of the Various PH Value on Structural and Magnetic Properties of Cobalt Ferrite Nanostructure

A.J. Mohammed [1], S.A. Hamdan[2]
[1,2] Department of Physics, College of Science, University of Baghdad, Baghdad, Iraq
[1] Ataaalbakri@gmail.com, suhadah22@gmail.com

A B S T R A C T

In this work, CoFe2O4 nanostructure was synthesized from Cobalt and ferric nitrates and sodium hydroxide (NaOH) by hydrothermal method. Effect of PH on the structural and magnetic properties of the resulting powder was studied at calcination 400°C and 600°C. The resulted products were characterized by X-ray diffraction (XRD), Field emission scanning electron microscopy (FE-SEM), Fourier transformed infrared (FTIR), and vibrating sample magnetometer (VSM) technique as synthesis , when calcination at 400°C and 600°C with different PH . The reduction in crystallite size that their average crystallite size is found (13.98-22.17) nm crystallite size at PH=9 higher than when PH=3. The FE-SEM images indicated that particles were agglomerated and spherical shape and size between (23.6 - 57.9) nm for PH=9 and (23.3 – 114.6) nm for PH=3. The created CoFe2O4 nanostructure have demonstrated ferromagnetic behavior for all the samples behavior which was found in VSM results examination.

Keywords: CoFe2O4 Nanoparticle, Hydrothermal Synthesis, Magnetic Properties

1. Introduction

Cobalt ferrite (CoFe2O4) is a significant member of the spinel ferrite family, characterized by its inverse spinel structure. In this structure, oxygen atoms form a face-centered cubic (FCC) lattice, while half of the Fe3+ ions occupy the tetrahedral a sites, and the remaining half, together with Co2+ ions, are situated at the octahedral B sites [1].

CoFe2O4 nanoparticles have been made using different methods, such as coprecipitation [2], microemulsion synthesis [3], sol-gel synthesis [4], and hydrothermal methods [5]. Typically, the aforementioned approaches necessitate the utilization of a metal salt and a potent base in order to facilitate the formation of the intended oxide. However, it should be noted that the dimensions and structure of the entity are highly susceptible to factors such as pH and temperature [6].

In this work, we have prepared CoFe2O4 samples using hydrothermal technique and characterized by XRD, FTIR, and FE-SEM. At room temperature, a vibrating sample magnetometer (VSM) was used to test the magnetic properties of CoFe2O4 samples that had been made. The investigation also looked at how pH and temperature affected the structure, morphology, and magnetic properties of the CoFe2O4 samples that were made.

*Corresponding author
E-mail address:

2. Experimental Work

CoFe2O4 nanostructure was prepared from Cobalt and ferric nitrates using the hydrothermal method. The aqueous solutions of Cobalt nitrate hexahydrate with 0.2M was dissolved in distilled water and stirred in a magnetic stirrer until the solution appears pink. Ferric nitrate monohydrates (Iron nitrate nanohadrate) with 0.4M was dissolved in distilled water and stirred it until the solution appears orange. Dissolve NaOH with (1, 2, and 3) M in deionized water and stirred at 70oC the resultant solution appears transparent. Then cobalt salt and iron salt were gradually added to NaOH boiled solution, then the pH of the solution was measured and its value was 3 and 9. The resultant solution stirred for (6h) at 70 oC, the solution appears black. The resulting solution was placed in an autoclave and then placed in an oven at 100 oC for (3h). Resulting solution centrifuged for 30 min with 6000 revolutions per minute, then this process was repeated three times. Dried the resulting precipitate at 100 oC for 30 min, the material appeared in the form of a small black mass. The resulting substance was ground well and became a black powder, then annealed at 400oC and 600oC the resulting samples are ready for examined .These same steps were repeated different concentrations of NaOH. In the present study, CoFe2O4 nanostructure have been prepared by using the hydrothermal technique and calcined at various temperatures (400, and 600) oC. The purpose of this work is to examine how the PH and calcination temperature affects morphological and structural of CoFe2O4 nanostructures synthesized. By using a Shimadzu version 4 (XRD) system, the structure related to the CoFe2O4 nanostructures was analyzed, and the intensity was recorded as a Bragg angle function. The radiation source was Cu (Kα) with λ= 1.5406 Å wavelength was used as the radiation source, while 40kV and 30mA were used for the voltage and current, respectively. The scanning angle 2θ was varied between 10 and 90 degrees step size 0.2 degree, at a speed of 10 degrees per min, with a preset time of 1.2 seconds. For analyzing the morphology regarding samples, a Field emission scanning microscope (FESEM) is used (MIRA3model-TE-SCAN (Dey Petronic Co.). The Fourier Transform Infrared (FTIR) test is employed to examine the spectra of various substances. This is achieved by utilizing a Bruker FTIR analyzer, specifically the Tensor-27 model, manufactured by Bruker Optics Inc. in Billerica, MA. The test is conducted in an attenuated total reflectance mode. The data were recorded within the 400–4000 cm-1 wave number range. An AGFM-VSM model 117 was used for recording M-H curves regarding the samples during magnetic experiments with the use of a VSM.

3. Results and Discussion

The cobalt ferrite nanostructure fabricated by employing a hydrothermal approach with 1 M of NaOH concentration, **PH is 9** and calcined for 0 ^{o}C, 400 ^{o}C and 600 ^{o}C are confirmed by the peaks observed (Fig. 1). The samples display the recognizable reflection from (220), (311), (222), (400), (422), (511), (440), and (533) planes, which are in good agreement with those of $CoFe_2O_4$ obtained from JCPDS card no. 96-591-0064. Another finding is that peaks shift to lower 2θ as the temperature of calcination rises, this shows that as thermal energy is added, the rate at which cobalt ions are incorporated into the lattice increases[7]. Due to the fact that the peak shift and lattice constant vary depending on the substituted cations, this makes it possible to discriminate between the diffraction patterns of distinct spinel ferrites[8]. However, when the calcination temperature increased, the peak strength steadily dropped, indicating that the expansion of peaks was hampered by the rise in calcination temperature. The vibrating of the atoms in the sample may be directly connected to the drop in nanoparticle peak intensity as temperature rises[9]. A recent study [10] has provided

evidence regarding the relationship between changes in the distance between adjacent crystal planes (referred to as d) and variations in atomic thermal vibration resulting from temperature increases. According to the study, the diffraction peak's 2 position shifts from its initial position as temperature rises, and the intensity of the diffraction peak decreases. The high purity of the product is supported by the fact that the XRD spectra did not find any further impurity peaks [11].

The determination of crystallite sizes in the ferrite-calcined samples was conducted by employing Debye-Scherrer's formula [12] [13], specifically focusing on the greatest intensity (311) peaks. The obtained results have been documented in Table 1.

$$D = \frac{k\lambda}{\beta \cos\theta} \quad (1)$$

Where k = shape factor, λ = 1.54060Å, β = Full Width Half Maximum (FWHM) and θ = diffracting angle. The results showed that when the calcination temperature increased, the crystallite sizes had relatively reduced. The high temperatures of the calcination process may be to blame for the nanoparticles' cracking or fracturing, which results in the reduction in crystallite size[14]. Using Bragg's Law, the lattice parameter was calculated from the XRD pattern [15]. The symbol for interplanar spacing is "d," and the lattice parameter for the corresponding 2 peak position value is "a." The integers h, k, and l are commonly referred to as Miller indices [16].

$$a = d\sqrt{h^2 + k^2 + l^2} \quad (2)$$

Lattice constant has expanded from 8.39 to 8.53 Å. The substituted cations affect how the lattice constant behaves since the radius of Fe^{3+} (0.64 Å) is lesser thanCo^{2+} (0.72 Å) this answers the rising lattice constant with the introduce of cobalt cation into the lattice. [17]. According to a research [8], the lattice constant increased as the calcination temperature rose.

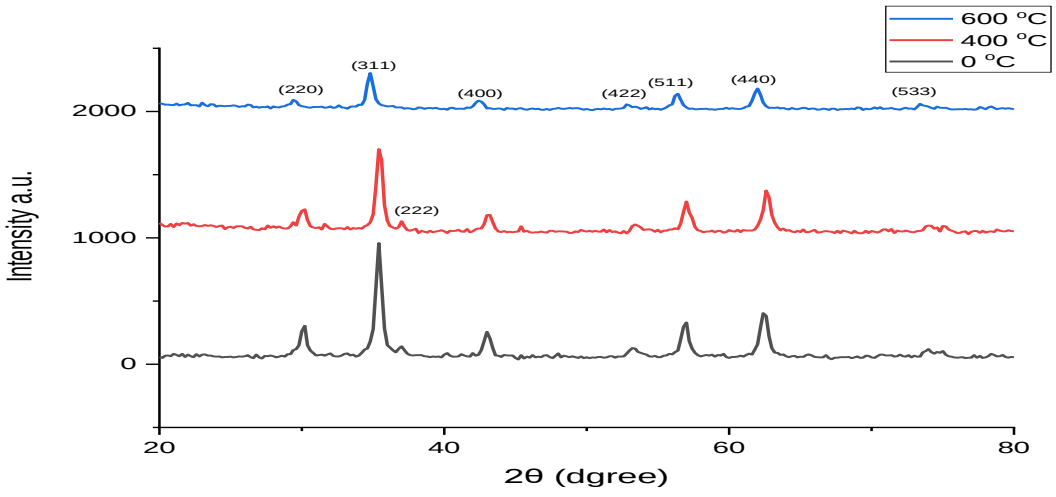

Figure 1: XRD of $CoFe_2O_4$ with different calcination temperature with pH is 9.

Figure (2) demonstrate the synthesized cobalt ferrite nanostructure by employing a hydrothermal technique with 1 M of NaOH concentration, **PH is 3** and calcined for 0 ^{o}C, 400 ^{o}C and 600 ^{o}C. The samples display the recognizable reflection from (311), (511), (440), and (622) planes, which are in good agreement with those of $CoFe_2O_4$ obtained from JCPDS card no. 96-591-0064. Peaks at 2θ 24.6^{o}, 33.6 ^{o}, 49.8 ^{o}, 54.4 ^{o} and 72.6^{o} is belong to hematite α-Fe_2O_3. Quyen *et al*[18] clarified the reason of the most peaks belong to hematite that the creation of iron hydroxide precursors is frequently at low pH solution and therefore the Fe/Co molar ratio in the final outcome increasing causes a rise the formation of α-Fe_2O_3 phase in the calcined products. Meanwhile Lafta *et al* [19]explain the low concentration of sodium hydroxide (low pH) leads the reaction to produce α-Fe_2O_3. Huang *et al* [20]also confirmed the with increase pH the hematite phase disappears. However, the peak strength gradually decreased as the calcination temperature rose, demonstrating that the increase in calcination temperature interfered with the growth of peaks. The decrease in nanoparticle peak intensity as temperature rises may be directly related to the atoms in the sample vibrating[9]. Recent research[10] shown how a rise in temperature-induced atomic thermal vibration might alter the distance between the closest crystal surfaces (d), and as a result, the diffraction peak's 2θ position changes from its initial position. The strength of the diffraction peak also reduces. The calculation of crystallite sizes was performed using Debye-Scherrer's formula (1) based on the (311) peaks. This analysis was conducted for all the ferrite-calcined samples, and the obtained results have been documented in Table 1. The findings demonstrated that the crystallite sizes had decreased as the calcination temperature rose. This could be due to the presence of α-Fe_2O_3 that was obtained by oxidation process[21]. Using Bragg's Law eq. (2), the lattice parameter was calculated from the XRD pattern. Lattice constant has expanded from 8.27 to 8.30 Å. Given that the radius of Fe^{3+} (0.64) is less than that of Co^{2+} (0.72), the substituted cations have an impact on how the lattice constant behaves, this answers the rising lattice constant with the introduce of cobalt cation into the lattice. [17]. In accordance with a study [8], as the calcination temperature climbed, the lattice constant increased.

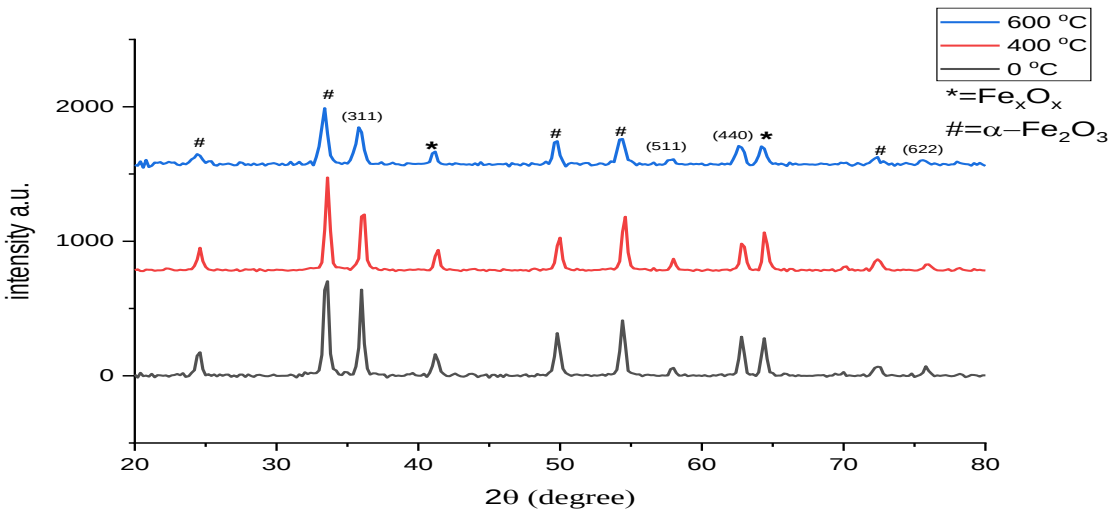

Figure 2: XRD of $CoFe_2O_4$ with different calcination temperature with pH is 3.

Table 1. Crystallite size and lattice constant of $CoFe_2O_4$ with different calcination temperature.

Sample Name	2θ(degree)	FWHM β	D(nm)	Lattice Constant

pH	Calcined Temperature °C		(degree)		(a) Å
9 pH	**0**	35.4226	0.6173	14.11	8.39
	400	35.468	0.6109	14.26	8.38
	600	34.8149	0.6218	13.98	8.53
3 pH	**0**	35.995	0.3936	22.17	8.27
	400	36.10637	0.5904	14.78	8.24
	600	35.83659	0.5904	14.77	8.3
JCPDS card		35.632			8.35

Figures (3 and 4) shows calcinated cobalt ferrite nanostructures at (0, 400 and 600) ^{o}C for (1 M) of NaOH concentration and pH is (3 and 9) presented in the range 4000-450 cm^{-1} have been investigated by FTIR spectroscopy at room temperature. The popular bands in the range3779-3426 cm^{-1}, 1637-1616 cm^{-1} and 1385cm^{-1} are assigned to the O–H stretching vibration demonstrating the presence of water adsorbed at the nanostructures' surface [22]–[29]. The absorption bands at 2922cm^{-1} were noticed, which are associated with C–H stretches[8], [23]. In addition, the frequency range of 583-562 cm^{-1} is associated with the metal-oxygen stretching vibrations occurring in the tetrahedral sites of spinel ferrites. Similarly, the frequency of 478 cm^{-1} corresponds to the metal-oxygen stretching vibrations in the octahedral sites of spinel ferrites. These findings have been reported in previous studies [15], [26], [30], [31]. The fabrication of cobalt ferrite uses different pH, as illustrated in Figures (3 and 4), which modifies absorption intensity while maintaining the same frequency range. This shows that cobalt ferrite manufacturing has the capacity to change its magnetic properties[32]. FTIR peaks of synthesized cobalt ferrite nanostructures were shown in Table (2).

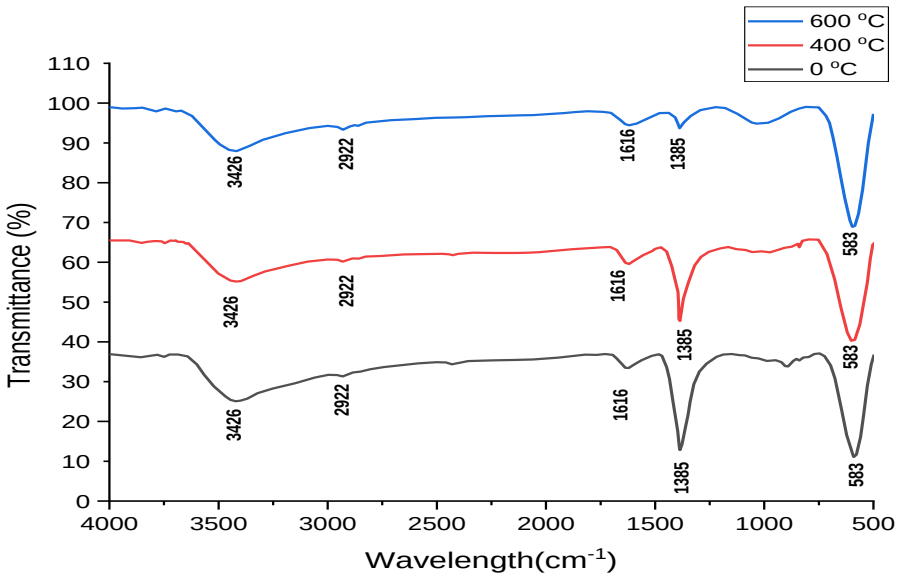

Figure 3: FTIR of $CoFe_2O_4$ with different calcination temperature with pH is 9.

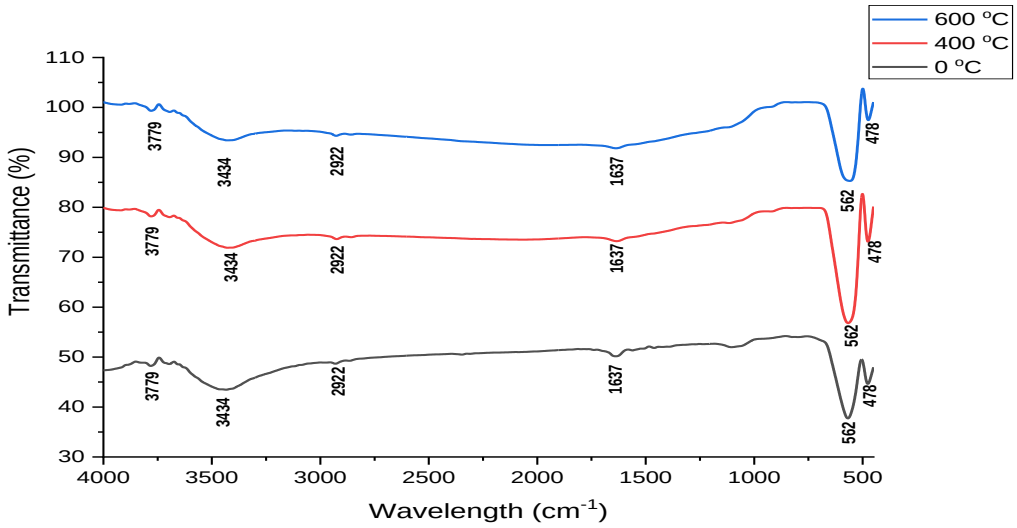

Figure 4: FTIR of $CoFe_2O_4$ with different calcination temperature with pH is 3.

Table 2: FTIR peaks of synthesized cobalt ferrite nanostructures.

Chemical Bonds	**Band Location cm^{-1}**	
	9 pH	3 pH
O–H stretching vibration		3779
O–H stretching vibration	3426	3434
C–H stretches	2922	2922
O–H stretching vibration	1616	1637
O–H stretching vibration	1385	
Metal-Oxygen stretching vibrations	583	587
Metal-Oxygen stretching vibrations		478

Figures (5, 6 and 7) shows the FE-SEM micrographs of cobalt ferrite nanostructure synthesized with 9 pH calcinated at different temperatures. The FE-SEM images indicated that particles were agglomerated and spherical shape and size between 23.6 to 57.9 nm. The observed particle size exhibited a greater magnitude compared to the crystallite size ascertained using the X-ray diffraction data. The resulting agglomeration caused multiple crystallites to come together to create a bigger particle due to a higher surface area to volume ratio. Also, due to grain expansion at higher calcination temperatures for the lowering of Gibbs free energy brought on by the reduction of expanded surface area of nanoparticles [15]. In addition, magnetic nanoparticles tend to cluster and stick together due to the interaction of magnetic dipoles[43] Similar results were observed in previous studies [40][39].

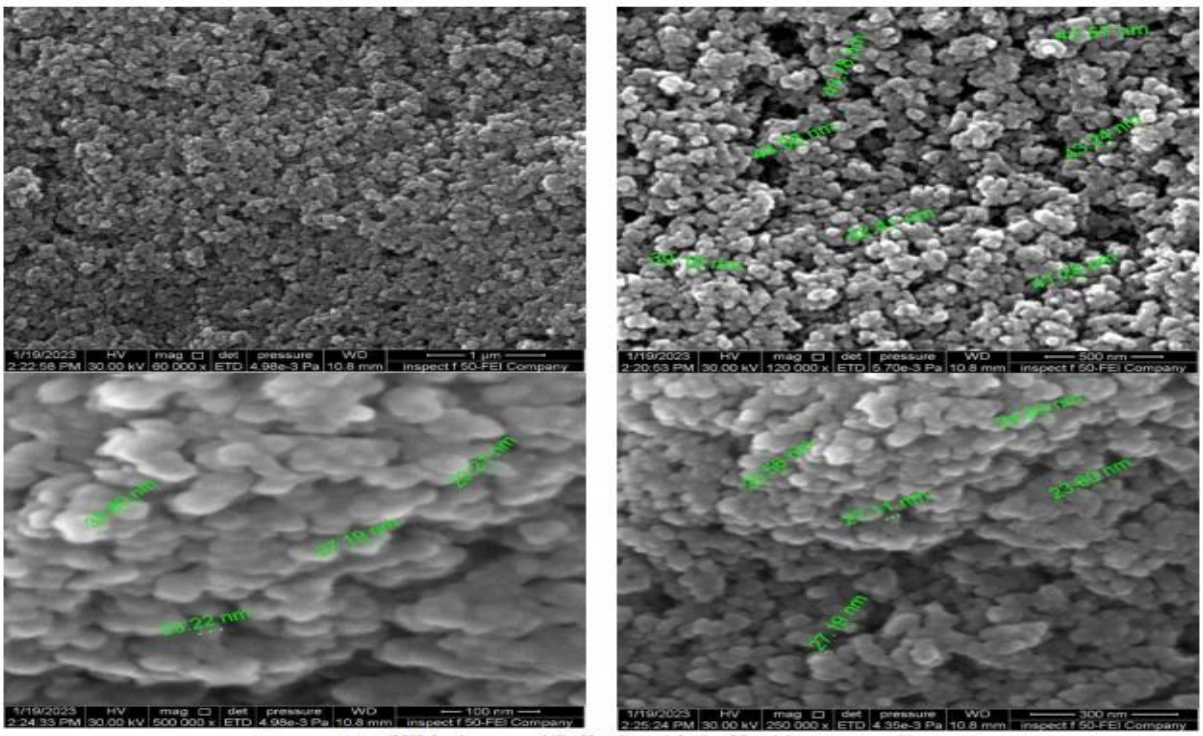

Figure (5): SEM picture of $CoFe_2O_4$ with 9 pH without annealing.

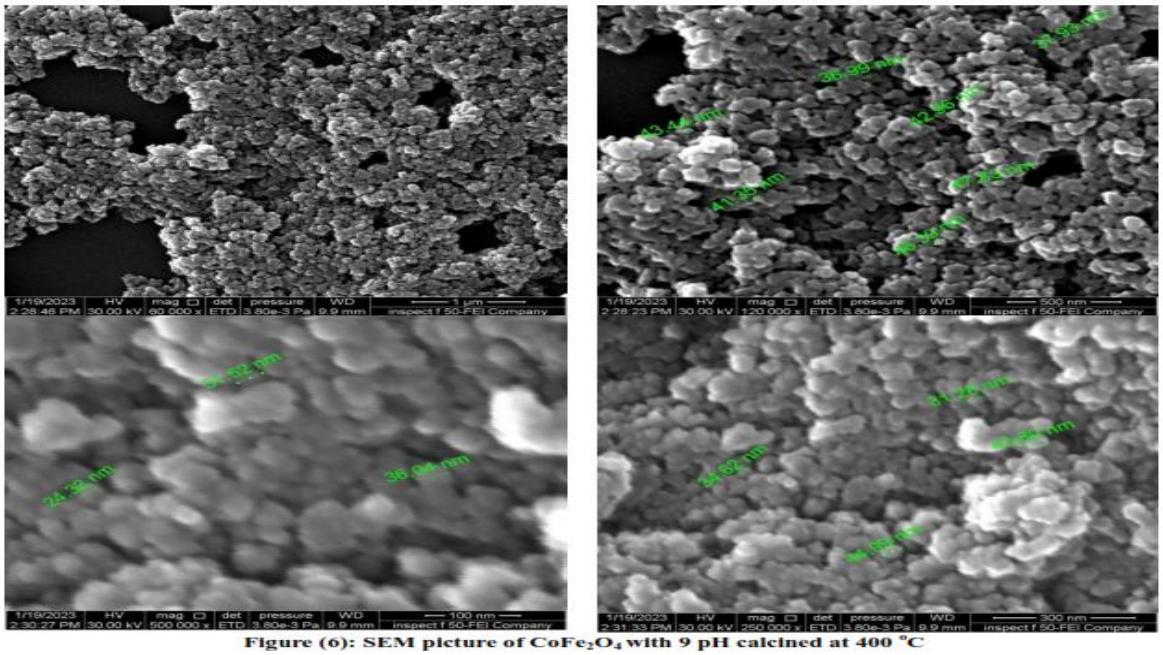

Figure (6): SEM picture of $CoFe_2O_4$ with 9 pH calcined at 400 °C

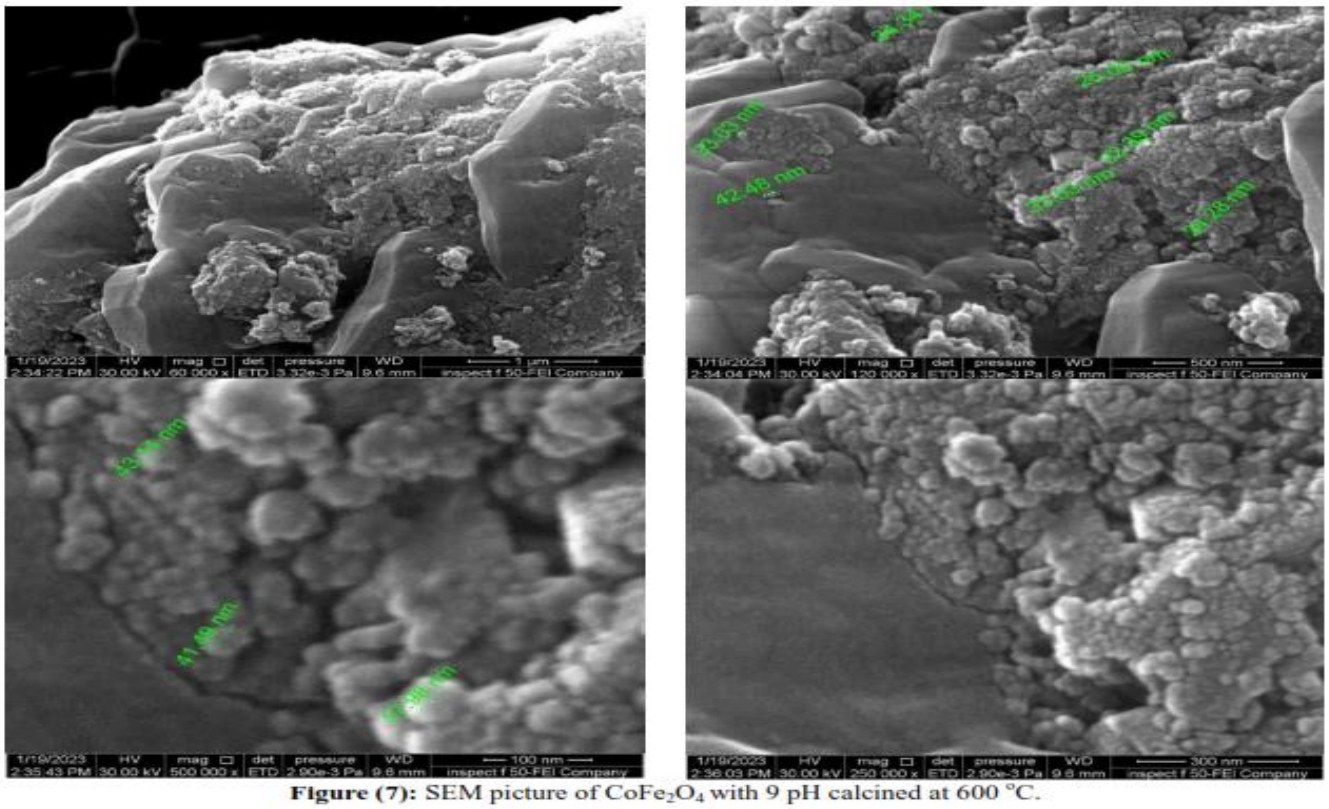

Figure (7): SEM picture of $CoFe_2O_4$ with 9 pH calcined at 600 °C.

Figures (8, 9 and 10) shows the FE-SEM micrographs of cobalt ferrite nanostructure synthesized with 3 PH calcinated at different temperatures. The FE-SEM images indicated that particles were agglomerated and spherical shape and size between 22.3 to 114.6 nm. The crystallite size determined from the X-ray diffraction data was less than the particle size that was actually observed. The resulting agglomeration caused multiple crystallites to come together to create a bigger particle due to a higher surface area to volume ratio. furthermore

due to the grain expansion at higher calcination temperatures for the minimization of Gibbs free energy as a result of the decrease of extended nanoparticle surface area[15]..Similar results were observed in previous studies[44][45].

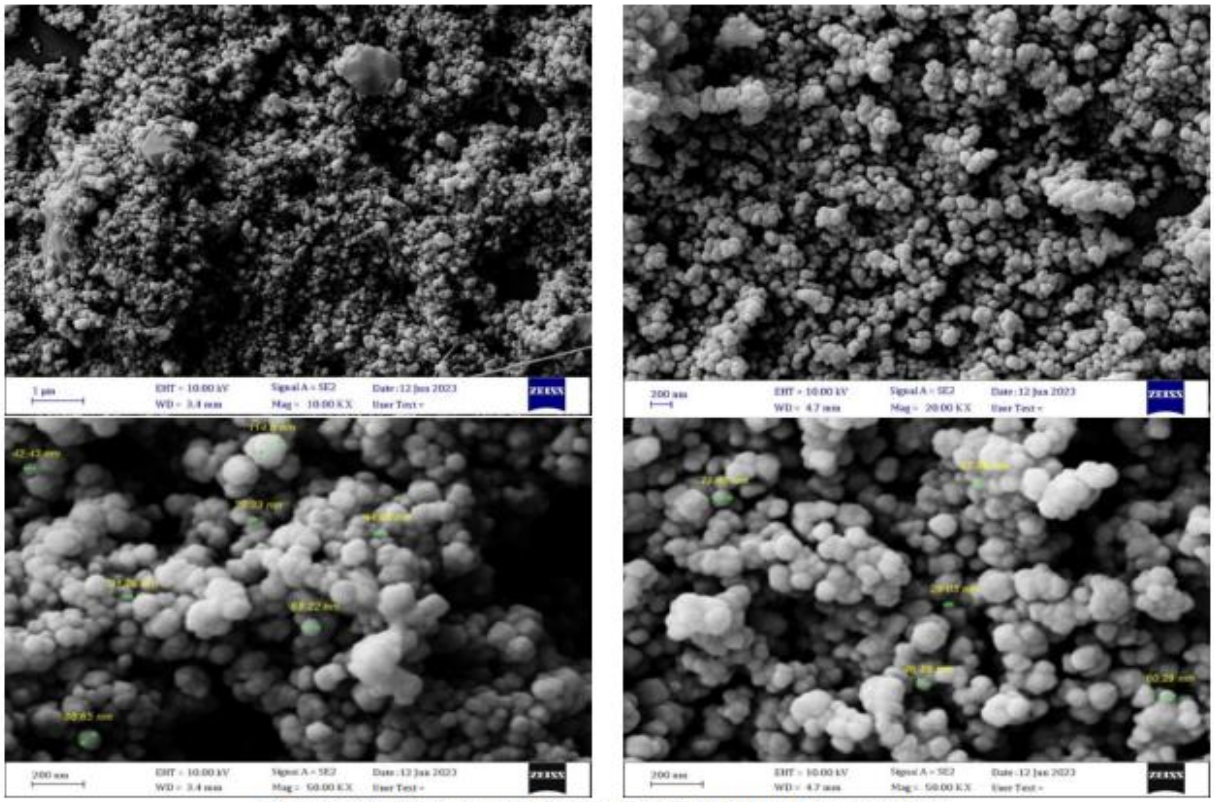

Figure (8): SEM picture of $CoFe_2O_4$ with 3 pH without annealing.

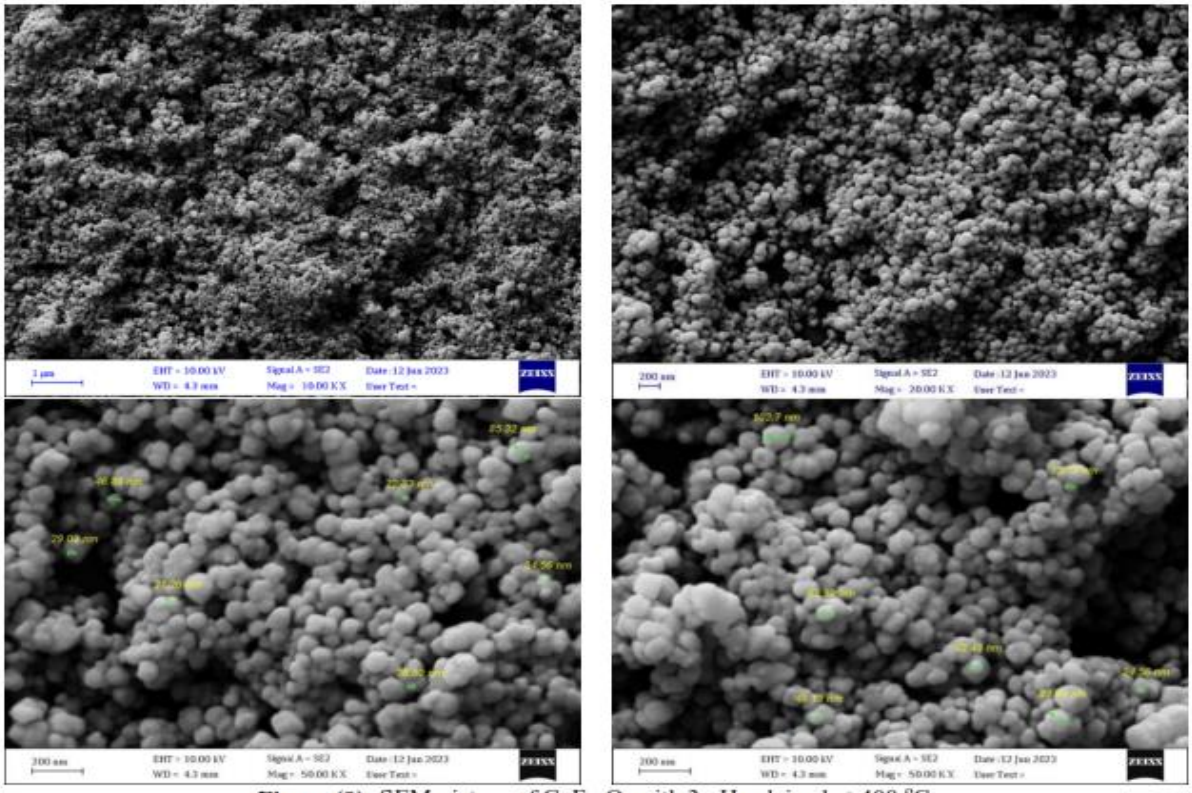

Figure (9): SEM picture of $CoFe_2O_4$ with 3 pH calcined at 400 °C.

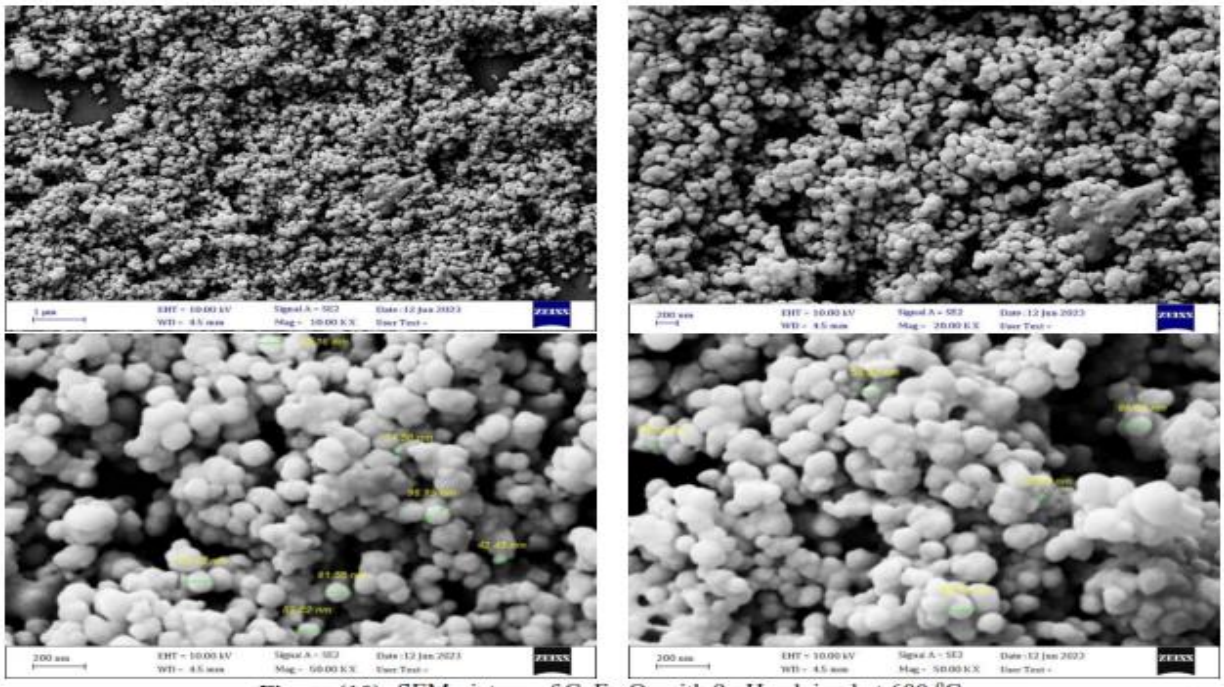

Figure (10): SEM picture of $CoFe_2O_4$ with 9 pH calcined at 600 °C.

Magnetic characterization of the cobalt ferrite synthesized with 9 pH samples before and after calcination was performed using a vibrating sample magnetometer (VSM) as showed in Figure (11). The discovered magnetic hysteresis at ambient temperature revealed that the

cobalt ferrite nanostructure has ferromagnetic characteristics both before and after calcination. The coercivity H_C of the $CoFe_2O_4$ nanostructure samples without annealing was 439 Oe, and after calcination for 400 and 600 ^oC, it increased to1740 and 1439 Oe respectively. The saturation magnetization (M_S) before calcination was 58 emu/g and after calcination it was 60 and 68 emu/g for 400 and 600 ^oC respectively. the saturation magnetization values (M_S) are lower than the bulk $CoFe_2O_4$ (~80 emu/g)[21][46]. The interplay between the magnetic spin moment's surface order and disorder and the disruption to the spinel structural inversion brought on by Laplace pressure may be responsible for this decrease in saturation magnetization[18]. Table 3 illustrates the relationship between calcination temperature and saturation magnetization (M_S) and remanent magnetization (M_R), indicating that both MS and MR exhibit an upward trend as the calcination temperature increases. This resulted from the treatment at low temperatures' partial crystallization and tiny particle size. SEM analysis has therefore verified that the particle size grew with increasing calcination temperature. The high number of surface atoms, the presence of unsaturated ligands, and the ability to cause significant thermal disturbances may also play a role. As a result, the crystal's magnetic structure was unstable and disordered, making it difficult to maintain the magnetic moment's consistency with the external field[44]. Additionally, because the amount of the non-magnetic layer on the powder surface dropped as the particle size increased, the saturation magnetization might rise as the particle size does as well [44]. Reduced grain growth is the cause of the rise in coercivity with increased calcining temperature[47].

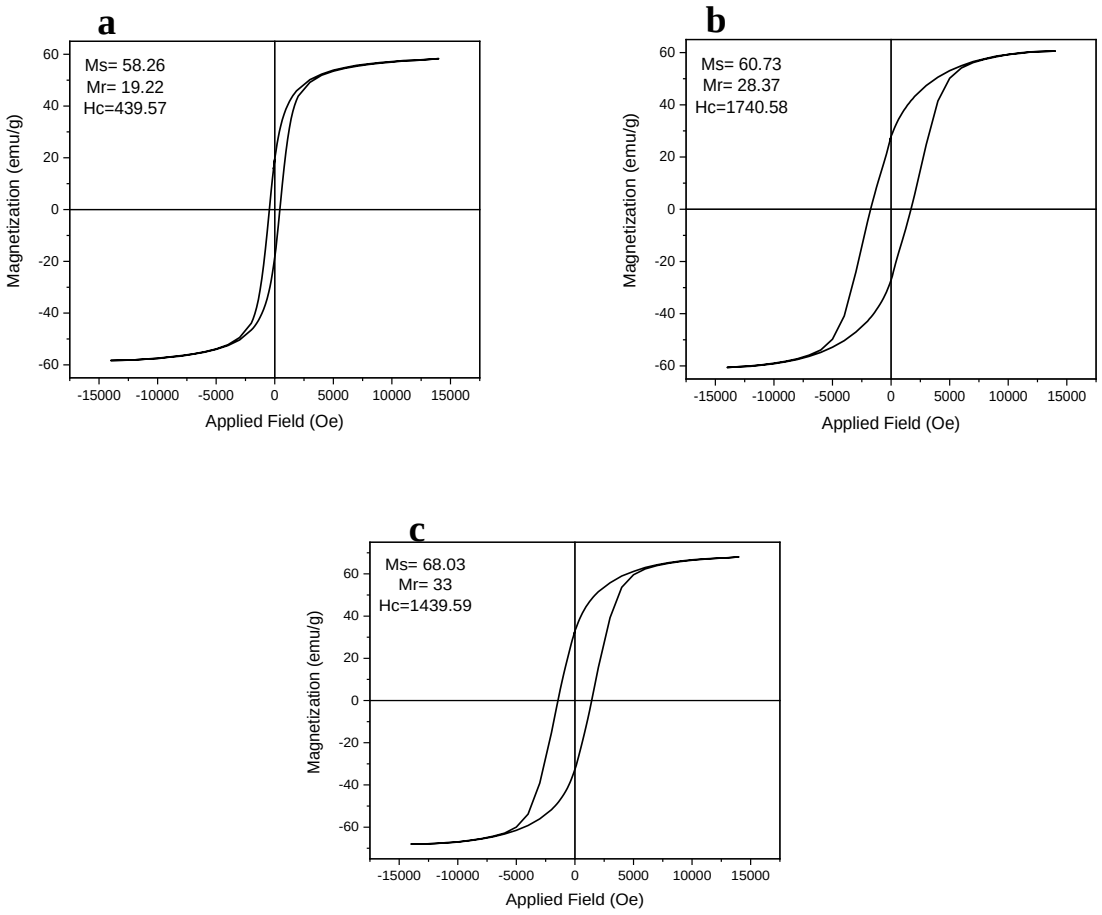

Figure 11: The hysteresis of M−H curve of $CoFe_2O_4$ with pH is 9 calcined at a: 0 ^oC, b:400 ^oC and c:600 ^oC.

Hysteresis loops were used to calculate the cobalt ferrite's magnetic characteristics. Fig. (12) shows the hysteresis loops of calcinated nanostructure at 0, 400 and 600 °C with 3 pH. Table (3) displays the H_C, M_S, and M_R data with low values. The presence of a spin structure that cancelled the zero magnetization caused by the canted spin order is indicated by a very modest magnetism [48]. Without calcination, the sample's low saturation magnetization value may have resulted from a little amount of Fe–O and O–Fe–O bond formation. However, as the calcination temperature was raised, the bond length and bond angle of the Fe–O and O–Fe–O bonds increased, which led to a drop in the magnetization value [49]. The fact that some grains do not have a spontaneous magnetic moment at higher temperatures means they are unable to contribute to the magnetization, which is another explanation for a drop in the value of magnetic saturation with rising calcination temperature[50] [51]. Due to the thermal variations of the blocked moment across the anisotropy barrier and the impossibility of the moments aligning in an applied field, H_C comparatively reduced with an increase in annealing temperature[21]. Remanent magnetization decreased with increment of calcined temperature due the process of saturation magnetization[52].

Table 3: Magnetic properties of the cobalt ferrite nanostructure.

Sample Name		Ms (emu/g)	Mr (emu/g)	H_C (Oe)
pH	**Calcined Temperature ^oC**			
	0	58.26	19.22	439.57
9 pH	**400**	60.73	28.37	1740.58
	600	68.03	33	1439.59
	0	0.5	0.108	1225.35
3 pH	**400**	0.38	0.055	914.97
	600	0.37	0.045	610.6

4. Conclusion

$CoFe_2O_4$ has been prepared through hydrothermal route successfully. After obtaining $CoFe_2O_4$ powders they were calcined at 400 ^oC and 500^oC. The nanocrystalline nature regarding the synthesized particles is confirmed by XRD data, and it was discovered that the crystallite size decrease at PH=9. Synthesized NPs had a spherical shape and size (23.6 -57.9) nm at PH=9 and (22.3-114.6) nm at PH=3 according to FESEM examination. Magnetic properties of $CoFe_2O_4$ nanostructure were investigated via VSM analysis. The magnetic saturation, magnetization remnant, and coercivity were all comparatively enhanced with PH=9. The hysteresis curves show normal ferromagnetic behaviour for all the samples.

5. References

[1] R. Valenzuela, *Magnetic Ceramics* (Cambridge University Press, Cambridge, 1994)

[2] J.P. Jolivet, C. Chanéac, P. Prené, L. Vayssières, E. Trone, J. Phys. IV France 7 (1997) C1-573–576.

[3] J.A. López Pérez, M.A. López Quintela, J. Mira, J. Rivas, S.W. Charles, J. Phys. Chem. B 101 (1997) 8045–8047.

[4] A.S. Albuquerque, J.D. Ardisson, W.A.A. Macedo, J. Magn. Magn. Mater. 192 (1999) 277–280.

[5] L. Diamandescu, D. Mihˇailˇa-Tˇarˇabˇa¸sanu, V. Teodorescu, N. Popescu-Pogrion, Mater. Lett. 37 (1998) 340–348.

[6] Linda J. Cote , Amyn S. Teja , Angus P. Wilkinson , Z. John Zhang , "Continuous hydrothermal synthesis of CoFe2O4 nanoparticles", Fluid Phase Equilibria 210 (2003) 307–317.

[7] L. Kumar and M. Kar, "Effect of La3+ substitution on the structural and magnetocrystalline anisotropy of nanocrystalline cobalt ferrite (CoFe2− xLaxO4)," *Ceram. Int.*, vol. 38, no. 6, pp. 4771–4782, 2012.

[8] Ermawati, F. U. (2021, November). XRD and EDX Analyses on the Formation of MgTiO3 Phase in (Mg0. 6Zn0. 4)(Ti0. 99Sn0. 01) O3 Powders Due to Calcination Temperature Variations. In *Journal of Physics: Conference Series* (Vol. 2110, No. 1, p. 012009). IOP Publishing.

[9] B. D. Cullity and S. R. Stock, "Elements of X-ray diffraction 3rd ed." Pearson Education Limited, 2014.

[10] Tataroglu, A. D. E. M., Buyukbas Ulusan, A., Altındal, Ş., & Azizian-Kalandaragh, Y. A. S. H. A. R. (2021). A compare study on electrical properties of MS diodes with

and without CoFe 2 O 4-PVP interlayer. *Journal of Inorganic and Organometallic Polymers and Materials*, *31*, 1668-1675.

[11] AL-Jawad, S. M., Taha, A. A., & Redha, A. M. (2019). Studying the structural, morphological, and optical properties of CuS: Ni nanostructure prepared by a hydrothermal method for biological activity. *Journal of Sol-Gel Science and Technology*, *91*, 310-323.

[12] Hamdan, S. A., & Ali, I. M. (2019). Enhancement of Hydrothermally Co3O4 Thin Films as H2S Gas Sensor by Loading Yttrium Element. *Baghdad Science Journal*, *16*(1), 221-229.

[13] abd Karem, I. K., & Hamdan, S. A. (2022). The Influence of CeO2 Concentration on Some Physical Properties of Y2O3 Thin Films. *Iraqi Journal of Science*, 2482-2491.

[14] Basak, M., Rahman, M. L., Ahmed, M. F., Biswas, B., & Sharmin, N. (2021). Calcination effect on structural, morphological and magnetic properties of nano-sized CoFe2O4 developed by a simple co-precipitation technique. *Materials Chemistry and Physics*, *264*, 124442.

[15] Ali, I. M., & Ibrahim, I. M. (2021). Toxic Gas Response for Nanostructured Cobalt Oxide Thin Films. *Iraqi Journal of Physics*, *19*(50), 20-30.

[16] Lan, N. T., Duong, N. P., & Hien, T. D. (2011). Influences of cobalt substitution and size effects on magnetic properties of coprecipitated Co–Fe ferrite nanoparticles. *Journal of Alloys and Compounds*, *509*(19), 5919-5925.

[17] H. T. K. N. Duong Hong Quyen, Dam Ngoc Anh, "Effect of Reaction pH on Characterization of Co-precipitated Cobalt ferrite Nanoparticles," *Int. J. Sci. Res. Sci. Eng. Technol.*, vol. 4, no. 8, 2018.

[18] Lafta, S. H. (2017). Effect of pH on structural, magnetic and FMR properties of hydrothermally prepared nano Ni ferrite. *Open Chemistry*, *15*(1), 53-60.

[19] Huang, X., Zhang, J., Wang, W., Sang, T., Song, B., Zhu, H., ... & Wong, C. (2016). Effect of pH value on electromagnetic loss properties of Co–Zn ferrite prepared via coprecipitation method. *Journal of Magnetism and Magnetic Materials*, *405*, 36-41.

[20] Moosavi, S., Zakaria, S., Chia, C. H., Gan, S., Azahari, N. A., & Kaco, H. (2017). Hydrothermal synthesis, magnetic properties and characterization of CoFe2O4 nanocrystals. *Ceramics International*, *43*(10), 7889-7894.

[21] J. Feng, R. Xiong, and Y. Liu, "Effect of NaOH Concentration and Adding Sequences on Structural and Magnetic Properties of Ni 0.4 Co 0.6 Fe 2 O 4 Nanopowders Prepared Via Co-precipitation Route," *J. Supercond. Nov. Magn.*, vol. 31, pp. 2079–2088, 2018.

[22] Jabbar, R., Sabeh, S. H., & Hameed, A. M. (2020). Synthesis and Characterization of CoFe2O4Nanoparticles Prepared by Sol-GelMethod. *Engineering and Technology Journal*, *38*(2B), 47-53.

[23] Malinowska, I., Ryżyńska, Z., Mrotek, E., Klimczuk, T., & Zielińska-Jurek, A. (2020). Synthesis of CoFe2O4 nanoparticles: the effect of ionic strength, concentration, and precursor type on morphology and magnetic properties. *Journal of Nanomaterials*, *2020*, 1-12.

[24] Márquez, G., Sagredo, V., Guillén-Guillén, R., Attolini, G., & Bolzoni, F. (2020). Calcination effects on the crystal structure and magnetic properties of CoFe2O4 nanopowders synthesized by the coprecipitation method. *Revista mexicana de física*, *66*(3), 251-257.

[25] Rahimi, Z., Sarafraz, H., Alahyarizadeh, G., & Shirani, A. S. (2018). Hydrothermal synthesis of magnetic CoFe 2 O 4 nanoparticles and CoFe 2 O 4/MWCNTs

nanocomposites for U and Pb removal from aqueous solutions. *Journal of Radioanalytical and Nuclear Chemistry*, *317*, 431-442.

[26] Refat, N. M., Nassar, M. Y., & Sadeek, S. A. (2022). A controllable one-pot hydrothermal synthesis of spherical cobalt ferrite nanoparticles: synthesis, characterization, and optical properties. *RSC advances*, *12*(38), 25081-25095.

[27] S. Pauline and A. P. Amaliya, "Synthesis and characterization of highly monodispersive CoFe2O4 magnetic nanoparticles by hydrothermal chemical route," *Arch. Appl. Sci. Res.*, vol. 3, no. 5, pp. 213–223, 2011.

[28] Agustina, A. K., Utomo, J., Suharyadi, E., Kato, T., & Iwata, S. (2018, May). Effect of synthesis parameters on crystals structures and magnetic properties of cobalt nickel ferrite nanoparticles. In *IOP Conference Series: Materials Science and Engineering* (Vol. 367, No. 1, p. 012006). IOP Publishing.

[29] Kumar, L., Kumar, P., Narayan, A., & Kar, M. (2013). Rietveld analysis of XRD patterns of different sizes of nanocrystalline cobalt ferrite. *International Nano Letters*, *3*, 1-12.

[30] Febriani, R. R., Prasetya, N. P., Wibowo, N. A., Supriyanto, A., Ramelan, A. H., & Purnama, B. (2023). Sodium-hydroxide molarities influence the structural and magnetic properties of strontium-substituted cobalt ferrite nanoparticles produced via co-precipitation. *Kuwait Journal of Science*.

[31] [32] D. E. Saputro, S. Budiawanti, S. W. Sukarsa, D. T. Rahardjo, and B. Purnama, "THE Agrawal, S., Parveen, A., & Azam, A. (2016). Structural, electrical, and optomagnetic tweaking of Zn doped CoFe2− xZnxO4− δ nanoparticles. *Journal of Magnetism and Magnetic Materials*, *414*, 144-152.

[32] Li, F., Kong, T., Bi, W., Li, D., Li, Z., & Huang, X. (2009). Synthesis and optical properties of CuS nanoplate-based architectures by a solvothermal method. *Applied Surface Science*, *255*(12), 6285-6289.

[33] Singh, A., Gangwar, H., & Dehiya, B. S. (2017). Synthesis and microstructural characterization of pure cobalt ferrite for DC electrical study. *J Mater Sci Mech Eng*, *4*, 136-141.

[34] Saleem, S., Irfan, M., Naz, M. Y., Shukrullah, S., Munir, M. A., Ayyaz, M., ... & Rahman, S. (2022). Investigating the impact of Cu2+ doping on the morphological, structural, optical, and electrical properties of CoFe2O4 nanoparticles for use in electrical devices. *Materials*, *15*(10), 3502.

[35] Al-Hada, N. M., Kamari, H. M., Baqer, A. A., Shaari, A. H., & Saion, E. (2018). Thermal calcination-based production of SnO2 nanopowder: an analysis of SnO2 nanoparticle characteristics and antibacterial activities. *Nanomaterials*, *8*(4), 250.

[36] Al-Hada, N. M., Kamari, H. M., Baqer, A. A., Shaari, A. H., & Saion, E. (2018). Thermal calcination-based production of SnO2 nanopowder: an analysis of SnO2 nanoparticle characteristics and antibacterial activities. *Nanomaterials*, *8*(4), 250.

[37] Habibi, M. H., & Parhizkar, H. J. (2014). FTIR and UV–vis diffuse reflectance spectroscopy studies of the wet chemical (WC) route synthesized nano-structure CoFe2O4 from CoCl2 and FeCl3. *Spectrochimica Acta Part A: Molecular and Biomolecular Spectroscopy*, *127*, 102-106.

[38] Dhiman, P., Sharma, G., Alodhayb, A. N., Kumar, A., Rana, G., Sithole, T., & ALOthman, Z. A. (2022). Constructing a Visible-Active CoFe2O4@ Bi2O3/NiO

Nanoheterojunction as Magnetically Recoverable Photocatalyst with Boosted Ofloxacin Degradation Efficiency. *Molecules*, *27*(23), 8234.

[39] L. Velayutham *et al.*, "Photocatalytic and antibacterial activity of CoFe2O4 nanoparticles from hibiscus rosa-sinensis plant extract," *Nanomaterials*, vol. 12, no. 20, p. 3668, 2022.

[40] A Kareem, H., Zaidi, M., Ameen Baqer, A., K Hachim, S., Ghazuan, T., Kadhim Alasedi, K., ... & MA Dahesh, S. (2022). Synthesis and Characterization of CoFe2O4 Nanoparticles and Its Application in Removal of Reactive Violet 5 from Water. *Journal of Nanostructures*, *12*(3), 521-528.

[41] Shahbahrami, B., Rabiee, S. M., & Shidpoor, R. (2020). Effect of pH Value on Synthesis and Properties of Zinc Cobalt Ferrite Nano Powders Prepared via Co-Precipitation Method.

[42] Hamad, H., Abd El-Latif, M., Kashyout, A. E. H., Sadik, W., & Feteha, M. (2015). Synthesis and characterization of core–shell–shell magnetic (CoFe 2 O 4–SiO 2–TiO 2) nanocomposites and TiO 2 nanoparticles for the evaluation of photocatalytic activity under UV and visible irradiation. *New Journal of Chemistry*, *39*(4), 3116-3128.

[43] Thomas, J., Thomas, N., Girgsdies, F., Beherns, M., Huang, X., Sudheesh, V. D., & Sebastian, V. (2017). Synthesis of cobalt ferrite nanoparticles by constant pH co-precipitation and their high catalytic activity in CO oxidation. *New Journal of Chemistry*, *41*(15), 7356-7363.

[44] Liu, Q., Sun, J., Long, H., Sun, X., Zhong, X., & Xu, Z. (2008). Hydrothermal synthesis of CoFe2O4 nanoplatelets and nanoparticles. *Materials Chemistry and Physics*, *108*(2-3), 269-273.

[45] Т. Р. Татарчук, "Structural, Optical, and Magnetic Properties of Zn-Doped CoFe2O4 Nanoparticles," 2017.

[46] F. A. Sulistiani, E. Suharyadi, T. Kato, and S. Iwata, "Effects of naoh concentration and temperature on microstructures and magnetic properties of bismuth ferrite (BiFeO3) nanoparticles synthesized by coprecipitation method," *Key Eng. Mater.*, vol. 855, pp. 9–15, 2020.

[47] H. Singh and J. K. Rajput, "Effect of calcination temperature on magnetic, structural, thermal and optical properties of BFO-T nanoparticles," *SN Appl. Sci.*, vol. 2, pp. 1–11, 2020.

[48] Y. Hu, L. Fei, Y. Zhang, J. Yuan, Y. Wang, and H. Gu, "Synthesis of bismuth ferrite nanoparticles via a wet chemical route at low temperature," *J. Nanomater.*, vol. 2011, pp. 1–6, 2011.

[49] F. Zhang, R. L. Su, L. Z. Shi, Y. Liu, Y. N. Chen, and Z. J. Wang, "Hydrothermal Synthesis of CoFe2O4 nanoparticles and their magnetic properties," in *Advanced Materials Research*, 2013, vol. 821, pp. 1358–1361.

[50] D. E. Saputro, U. Utari, and B. Purnama, "Effect of bismuth substitution on magnetic properties of CoFe2O4 nanoparticles: Study of synthesize using coprecipitation method," *J. Phys. Theor. Appl*, vol. 3, no. 9, 2019.